THE ASTROPHYSICAL JOURNAL, 600:88–95, 2004 January 1

DISTRIBUTION OF FARADAY ROTATION MEASURE IN JETS FROM ACTIVE GALACTIC NUCLEI. I. PREDICTIONS FROM OUR SWEEPING MAGNETIC TWIST MODEL

YUTAKA UCHIDA,[1,2] HIROMITSU KIGURE,[1,3] SHIGENOBU HIROSE,[1,4] MASANORI NAKAMURA,[1,5] AND ROBERT CAMERON[1,6]
Received 2002 November 9; accepted 2003 September 9

ABSTRACT

Using the numerical data of MHD simulation for active galactic nucleus (AGN) jets based on our "sweeping magnetic twist model," we calculated the Faraday rotation measure (FRM) and the Stokes parameters to compare with observations. We propose that the FRM distribution can be used to discuss the three-dimensional structure of magnetic field around jets, together with the projected magnetic field derived from the Stokes parameters. In the present paper, we assumed the basic straight part of the AGN jet and used the data of axisymmetric simulation. The FRM distribution that we derived has a general tendency to have gradient across the jet axis, which is due to the toroidal component of the helical magnetic field generated by the rotation of the accretion disk. This kind of gradient in the FRM distribution is actually observed in some AGN jets, which suggests a helical magnetic field around the jets and thus supports our MHD model. Following this success, we are now extending our numerical observation to the wiggled part of the jets, using the data of three-dimensional simulation based on our model, in an upcoming paper.

Subject headings: galaxies: jets — galaxies: magnetic fields — MHD — polarization

1. INTRODUCTION

Various models have been proposed to explain the formation of active galactic nucleus (AGN) jets and other astrophysical jets. Among them, the magnetohydrodynamic (MHD) model is one of the most promising models, since it can explain both the acceleration and the collimation of the jets. Lovelace (1976) and Blandford (1976) first proposed the magnetically driven jet from accretion disks, and Blandford & Payne (1982) discussed magneto-centrifugally driven outflow from a Keplerian disk in steady, axisymmetric, and self-similar situations. Uchida & Shibata (1985) performed a time-dependent, two-dimensional, axisymmetric simulation in the case of star-forming outflows. They pointed out that large-amplitude torsional Alfvén waves (TAWs) generated by the interaction between the accretion disk and a large-scale magnetic field play an important role (details are described in § 2). In this paper, we refer to this model as the "sweeping magnetic twist model." Uchida & Shibata (1986) extended the treatment to the case of AGN jets. Following this work, many authors have performed time-dependent, two-dimensional, axisymmetric simulations (e.g., Stone & Norman 1994; Ustyugova et al. 1995; Matsumoto et al. 1996; Ouyed & Pudritz 1997; Kudoh, Matsumoto, & Shibata 1998). Acceleration mechanisms in MHD models were studied in detail by using 1.5-dimensional MHD equations (Kudoh & Shibata 1997a, 1997b).

Using the numerical data of MHD models, observational quantities such as the Faraday rotation measure (FRM) or the Stokes parameters have been derived to compare to observations of AGN jets: Laing (1981) computed the total intensity, linear polarization, and projected magnetic field distributions, assuming some simple magnetic field configurations and high-energy particle distributions in the cylindrical jet. Clarke, Norman, & Burns (1989) performed two-dimensional MHD simulations, in which a supersonic jet with a dynamically passive helical magnetic field was computed, and derived distributions of the total intensity, projected electric field, and linear polarization.

Hardee & Rosen (1999) calculated the total intensity and the projected magnetic field distributions, using three-dimensional MHD simulations of strongly magnetized conical jets. Hardee & Rosen (2002) calculated the FRM distribution and argued that the observation of the radio source 3C 465 in Abell cluster A2634 (Eilek & Owen 2002) suggests helical twisting of the flow.

The FRM is given by the integral of $n_e B_\parallel$ along the line of sight between the emitter and the observer (where $B_\parallel$ is the line-of-sight component of the magnetic field and n_e is the electron density there). It is, in principle, not possible to specify which part of the line of sight the contribution comes from. However, in recent high-resolution radio observations (e.g., Eilek & Owen 2002; Asada et al. 2002), the FRM distribution seems to have good correlation with the configuration of the jet; this suggests that the FRM variation is due to the magnetized thermal plasma surrounding the emitting part of the jet. In fact, sharp FRM gradients seen in 3C 273 cannot be produced by a foreground Faraday screen (Taylor 1998; Asada et al. 2002). If this is the case, we can get new information, that is, the line-of-sight component of the magnetic field, and thus can predict the three-dimensional configuration of the magnetic field around the jet, together with the projected magnetic field.

In this paper, we calculate the FRM, projected magnetic field, and total intensity from the numerical data of MHD simulation based on our "sweeping magnetic twist model," and discuss these model counterparts comparing with some observations. Here we consider the straight part of the jet, and thus use the data of axisymmetric simulation. In § 2, we review the physics of our "sweeping magnetic twist model." We

[1] Department of Physics, Tokyo University of Science, 1-3 Kagurazaka, Shinjuku-ku, Tokyo 162-8601, Japan.
[2] Deceased, August 17, 2002.
[3] Kwasan and Hida Observatories, Kyoto University, Yamashina, Kyoto 607-8471, Japan; kigure@kwasan.kyoto-u.ac.jp.
[4] Department of Physics and Astronomy, Johns Hopkins University, Baltimore, MD 21218-2686.
[5] Jet Propulsion Laboratory, California Institute of Technology, 4800 Oak Grove Drive, Pasadena, CA 91109.
[6] Max-Planck-Institut für Astronomie, Max-Planck-Strasse 2, D-37191 Katlenburg-Lindau, Germany.

introduce the method to calculate model counterparts of observational quantities in § 3, and show the results in § 4. Comparisons of model counterparts with some observations are discussed in § 5.

2. BRIEF REVIEW OF OUR SWEEPING MAGNETIC TWIST MODEL

In this section, we briefly review the results of 2.5-dimensional MHD simulations based on our "sweeping magnetic twist model" to discuss the magnetic field around the straight part of jets. In an upcoming paper, we will extend our treatment to the wiggled part of jets, which we have given an interpretation using a three-dimensional MHD simulation based on our model (Nakamura, Uchida, & Hirose 2001).

In the original MHD model for bipolar outflows in star-forming regions, Uchida & Shibata (1985) considered a gravitational contraction of magnetized gas to form a star (plus an accretion disk). They attributed the large-scale magnetic field to the weak field in the Galactic arms. It is strengthened in the process of gravitational contraction of the interstellar gas to the star-forming core and plays a critical role. The toroidal field is continuously produced from the poloidal field by the rotation of the accretion disk. This causes magnetic braking to the disk material, and the material that loses angular momentum falls gradually toward the central gravitator and releases the gravitational energy. A part of the released gravitational energy is supplied to the jets along the magnetic field. The produced toroidal magnetic field propagates in two directions along the bunched large-scale magnetic field as large-amplitude TAWs. These TAWs serve to collimate the large-scale poloidal field into the shape of a slender jet by dynamically pinching it during the propagation ("sweeping pinch effect"). This process, verified in the simulation, was proposed by Uchida & Shibata (1985) as a generic magnetic effect operating in the formation of astrophysical jets utilizing gravitational energy.

The mechanism was applied to the case of AGN jets (Uchida & Shibata 1986) by supposing that a large-scale intergalactic magnetic field plays the role in the case of the formation of a protogalaxy and a giant black hole at its core. They argued that the same process as in the star formation case is applicable to the AGN jet cases, with more or less similar setup (having accretion disk around the central gravitator etc.), as a result of the similarity of the basic equation system. One of the possible differences between AGN jets and star formation jets may be the relativistic effects. The effect of general relativity is appreciable very close to the central giant black hole, which means that it is appreciable when the distance from the black hole is comparable to the Schwarzschild radius (Koide, Shibata, & Kudoh 1998). There are regions in which the special relativity should be taken into account, when the Alfvén velocity estimated in the classical definition is close to or exceeds the velocity of light. Here in this paper, we concentrate on the essential physical process in the production and collimation of the jet in the nonrelativistic range.

The problem was treated with the nonlinear system of MHD equations in a time-dependent way for the first time when Uchida & Shibata proposed this model in 1985. The numerical approach was the so-called axial 2.5-dimensional approximation, in which the quantities are axisymmetric, but the azimuthal components of vectors are included to allow them to play very essential roles, such as the centrifugal effect or pinch effect. Thus, the authors were able to deal with the physical driving and collimating mechanism they proposed to be in operation for astrophysical jets.

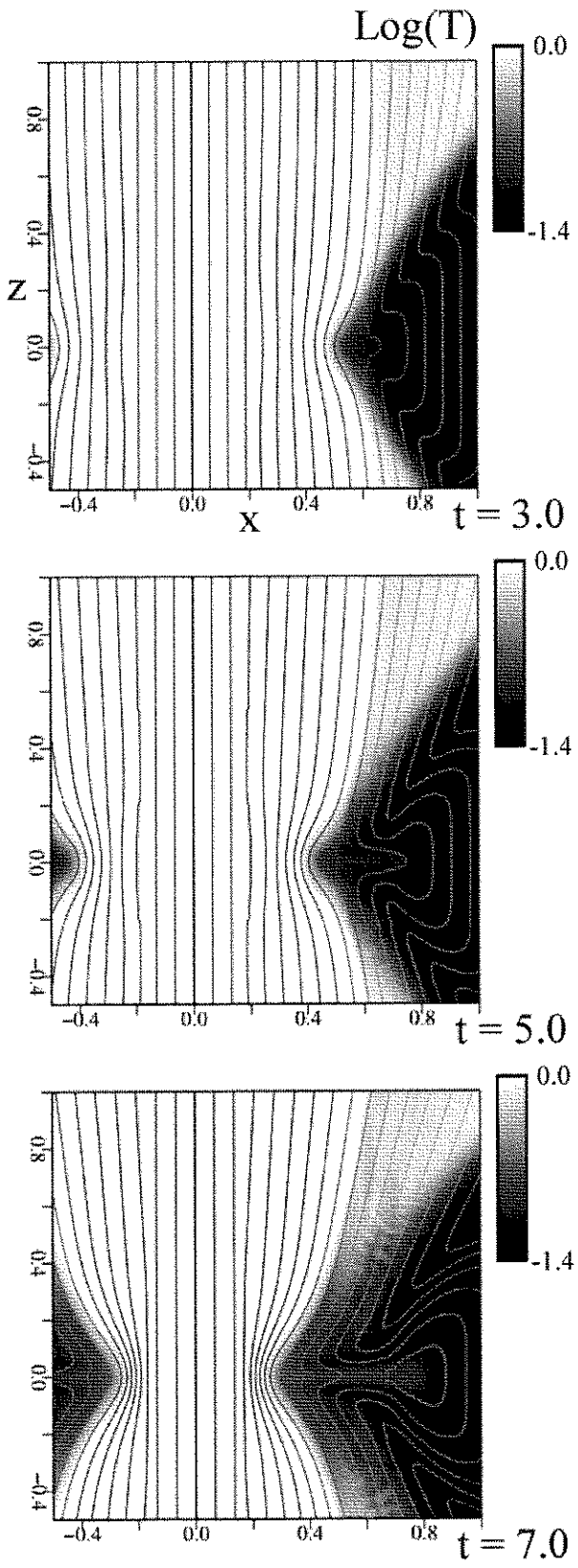

FIG. 1.—Time development in the r-z plane in our 2.5-dimensional MHD simulation near the central core. The distribution of logarithmic temperature is shown in gray scale. Curves represent the poloidal magnetic field.

Figure 1 shows the time development in the 2.5-dimensional MHD simulation based on our model. The rotating gas pulls the magnetic field gradually inward, which twists up the magnetic field, because the rotational velocity is faster closer to the center (Fig. 2). This continuously supplies large-amplitude TAWs (Poynting flux) along the external magnetic field, which pinch the poloidal magnetic field into the shape of a slender jet, as discussed above. The gas in the surface of the torus is swirled out in two directions along the axis, by both the magnetic pressure gradient and the centrifugal effect. Thus, the propagation of the TAW accelerates the gas in the surface of the disk into the spinning jets.

It is noted that the accretion toward the central gravitator takes place in the form of avalanches from upper and lower surfaces of the geometrically thick torus (Matsumoto et al. 1996), because the transfer of angular momentum to the external magnetic field is most efficient there. The magnetic fields of opposite polarity, brought with the accretion flows avalanching on the surfaces of the disk, allow a reconnection at the innermost edge of the disk in the equatorial plane (Fig. 1). This process contributes the supply of the "seed high-energy particles" into the jet. Such particles are reaccelerated through the Fermi-I acceleration process, in which two TAW fronts trapping the particles in between them approach each other, for example, as the foregoing one is decelerated as a result of an encounter with a high-density gas blob remaining in the collapse (Uchida et al. 1999).

3. METHOD OF CALCULATION OF MODEL COUNTERPARTS

Using the numerical data of the 2.5-dimensional simulation explained in the previous section, we computed the distribution of the FRM with some viewing angles. We also calculated the distributions of the projected magnetic field and the total intensity.

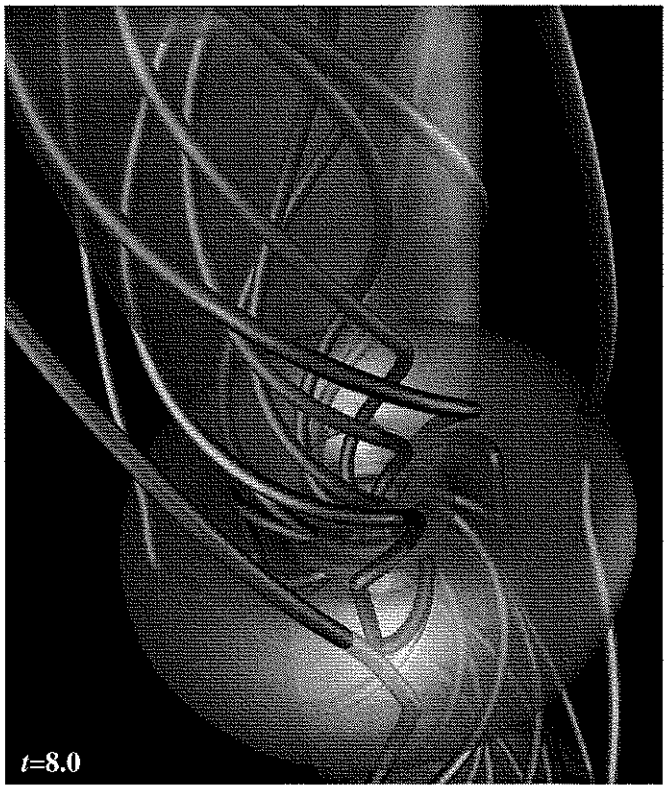

FIG. 2.—Three-dimensional presentation of the magnetic field with the accretion torus and jets (Meier, Koide, & Uchida 2001).

We computed the FRM distribution by integrating $n_e B_\parallel$ along the line of sight (Hardee & Rosen 2002). To calculate the Stokes parameters, we assumed the following: (1) the radiation process is synchrotron radiation, (2) synchrotron self-absorption is negligible, (3) the spectral index, α, is equal to unity, and (4) the projected magnetic field is perpendicular to the projected electric field. The emissivity of the synchrotron radiation is given by $\epsilon = p|B \sin \psi|^{\alpha+1}$, where B is the local magnetic field strength, ψ is the angle between the local magnetic field and the line of sight, and p is the gas pressure. In our simulation the relativistic particles were not explicitly tracked; therefore, we assumed that the energy and number densities of the relativistic particles are proportional to the energy and number densities of the thermal fluid (Clarke et al. 1989; Hardee & Rosen 1999, 2002). The total intensity is then given by the integration of the emissivity along the line of sight as $I = \int \epsilon \, ds$. Other Stokes parameters are given by $Q = \int \epsilon \cos 2\chi' \, ds$ and $U = \int \epsilon \sin 2\chi' \, ds$, where the local polarization angle χ' is determined by the direction of the local magnetic field and the direction of the line of sight. Using these U and Q, the polarization angle χ is given by $\chi = (1/2) \tan^{-1}(U/Q)$. Finally, the projected magnetic field is determined from the polarization angle χ and the polarization intensity $(Q^2 + U^2)^{1/2}$.

Here we separated the Faraday rotation screen and the emitting region, and we performed the integrations only in the emitting region for the Stokes parameters and the Faraday rotation screen for the FRM. We assumed this separation on the basis of the linear dependence of the observed polarization angle on wavelength-squared holds in some observations (Perley, Bridle, & Willis 1984; Feretti et al. 1999; Asada et al. 2002); this would not be the case if the Faraday rotation were caused in the emitting region (Burn 1966). Figure 3 shows the emitting region (*the region in the box of dashed lines*) and the Faraday rotation screen (*the region in the box of dotted lines*) assumed in our calculations. The cylindrical shell outside the emitting region is assumed to play the main role of the Faraday rotation screen, because the temperature is lower and the toroidal field is stronger there (Fig. 3) than in the tenuous clouds in the intergalactic space.

We consider two types of emitting regions: one is the layer type (type L: high-energy particles that exist only in the surface part of the dashed box in Fig. 3*a*) and the other is the column type (type C: high-energy particles that fill the whole region of the dashed box). The former corresponds to the idea that the high-energy particles are injected into the innersurface part of the jet because of the magnetic reconnection at the inner edge of the accretion disk as described in § 2. The latter may happen if the high-energy particles come from the pair plasma creation in the black hole magnetospheres.

4. RESULTS OF NUMERICAL OBSERVATIONS

4.1. *Faraday Rotation Measure*

The model counterparts of the FRM distribution with different viewing angles are shown in Figure 4. When we see the jet from the direction perpendicular to its axis ($\theta = 90°$, where θ is the angle between the jet axis and the line of sight), we see only the toroidal component of the helical field, and thus the value of the FRM is almost *antisymmetric* with respect to the axis (it is not perfectly antisymmetric because the radial

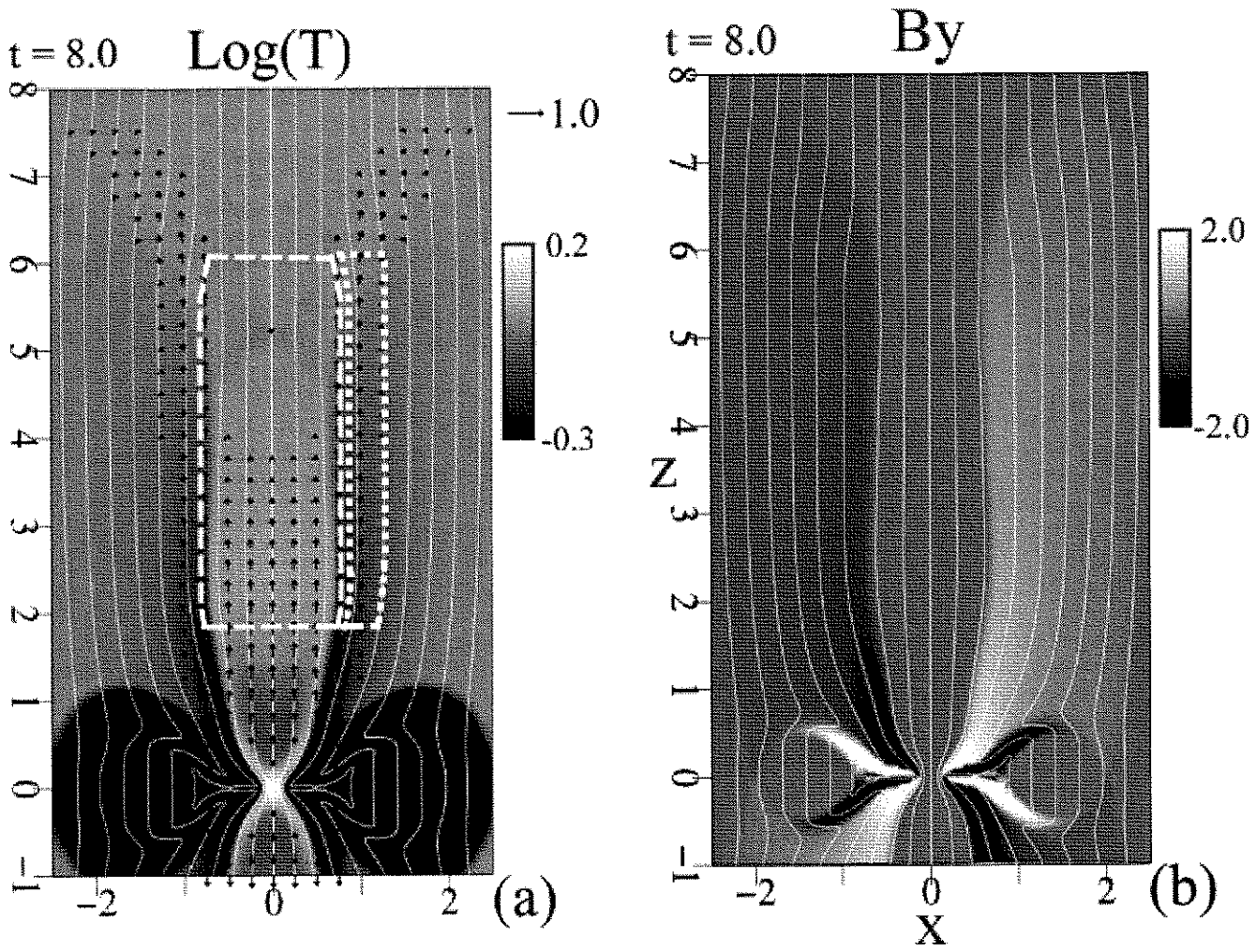

FIG. 3.—(*a*) Distribution of logarithmic temperature (*gray scale*; *dark represents the lower temperature*), together with the poloidal field (*white curves*) and poloidal velocity field (*arrows*) in the x-z plane. The white box with dotted lines and that with dashed lines are assumed to be the Faraday rotation screen and the emission region, respectively. (*b*) Poloidal magnetic field and toroidal magnetic field (B_y) (*gray scale*; *white represents plus and dark represents minus*).

component of the magnetic field is not equal to zero). The distribution of the FRM is distorted from antisymmetry as the viewing angle varies, but it *always shows gradient across the jet axis* (Fig. 4, row 2); this gradient across the jet axis can be interpreted as the sum of the antisymmetric part due to the toroidal component of the helical field and a base value due to the longitudinal component. When $|\theta - 90^\circ|$ is larger than the pitch angle of the helical field, this longitudinal component dominates (Fig. 4, row 1).

4.2. *Projected Magnetic Field and Total Intensity*

Figure 5 shows the distributions of the projected magnetic field and the total intensity with different viewing angles in the case of the type-L–emitting region. When θ is equal to 90°, the total intensity is nearly constant but has an edge-brightening; this is because the emissivity becomes smaller farther away from the axis, and the integration depth of the emitter has a maximum at edges. In other cases, the distribution of the total intensity is asymmetric, since the emissivity changes as $|\sin(\theta - \zeta)|^{\alpha+1}$ at the left edge and $|\sin(\theta + \zeta)|^{\alpha+1}$ at the right edge, where ζ is the pitch angle of the clockwise (seen from the jet origin) helical field.[7] Therefore, for example, it becomes dark at the left edge when θ is nearly equal to ζ. As for the projected magnetic field, it is perpendicular to the jet axis in the almost entire region, which does not depend on the viewing angle. This is because the the toroidal magnetic field is dominant in the emitting region.

Figure 6 shows the distributions in the case of the type-C–emitting region. In this case, the intensity has the peak on the axis when $\theta = 90^\circ$, because the integration depth has a maximum at the center of the jet. When the viewing angle is not so small, the projected magnetic field is parallel to the jet axis, which corresponds to the poloidal magnetic field in the emitting region. When the viewing angle is small (e.g., $\theta = 15^\circ$), the distributions of the total intensity and the projected magnetic field are almost the same as those in type L. This is because the fraction of the magnetic field perpendicular to the line of sight, which contributes to the synchrotron radiation, is small in both cases.

5. SUMMARY AND DISCUSSION

We calculated the FRM and the Stokes parameters using numerical data of 2.5-dimensional MHD simulation based on our sweeping magnetic twist model. The distribution of the FRM always has a gradient across the jet axis, which is caused by the toroidal magnetic field generated by the disk rotation. In

[7] Note that this is the opposite sense of that shown in Fig. 2.

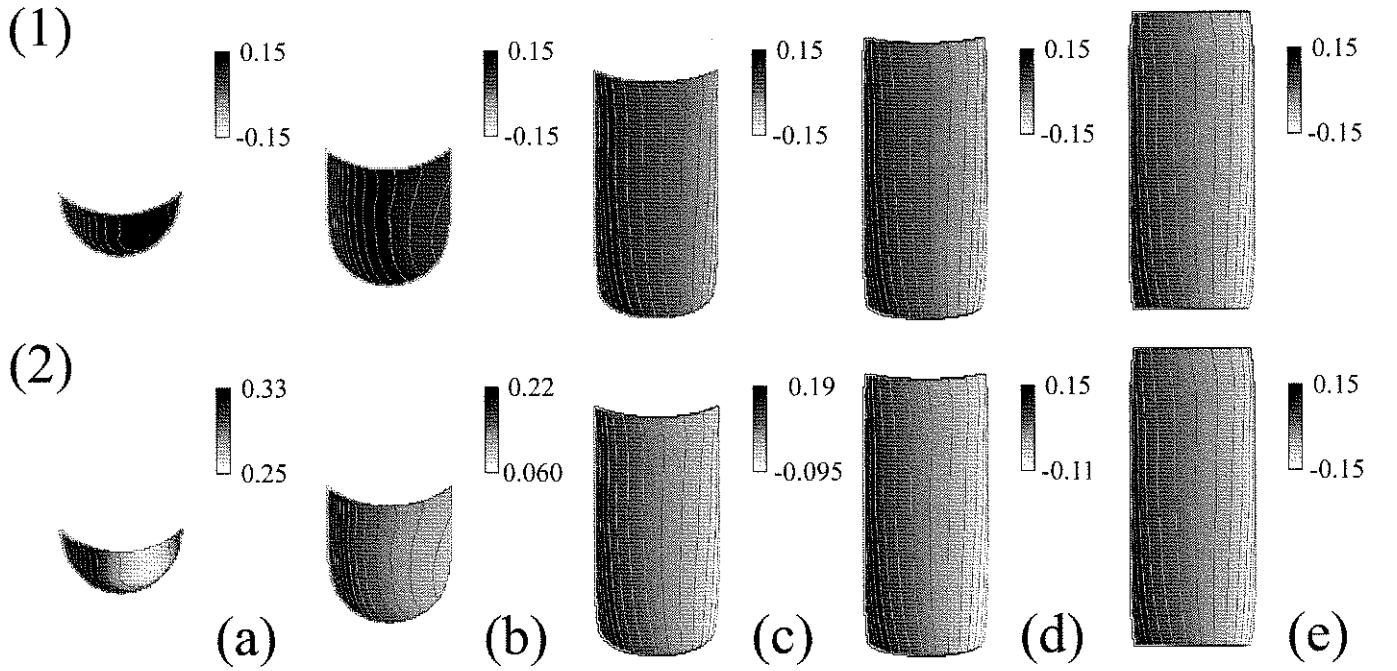

FIG. 4.—Calculated model counterparts for the FRM distribution, when seen at (*a*) 15°, (*b*) 30°, (*c*) 60°, (*d*) 75°, and (*e*) 90° from the axis (ahead of the jet). Only those corresponding to the upper part of the jet ($z > 0$) are shown. The direction of the jet coincides with that of the longitudinal magnetic field. The gray-scale range of the FRM distribution is fixed in the first row, while it is determined in each viewing angle in the second row. The accretion disk is the lower side in these pictures.

calculating the Stokes parameters, we assumed two types of emitting regions, the column type and the layer type. In the former, the projected magnetic field tends to be parallel to the jet axis and the total intensity peaks at the jet center. On the other hand, in the latter, the projected magnetic field is perpendicular to the axis; the total intensity has "edge-brightening," which is observed in Cen A (Clarke, Burns, & Feigelson 1986) and M87 (Biretta, Owen, & Hardee 1983; Junor, Biretta, & Livio 1999). In the following, we discuss the three-dimensional magnetic field structure around the observed

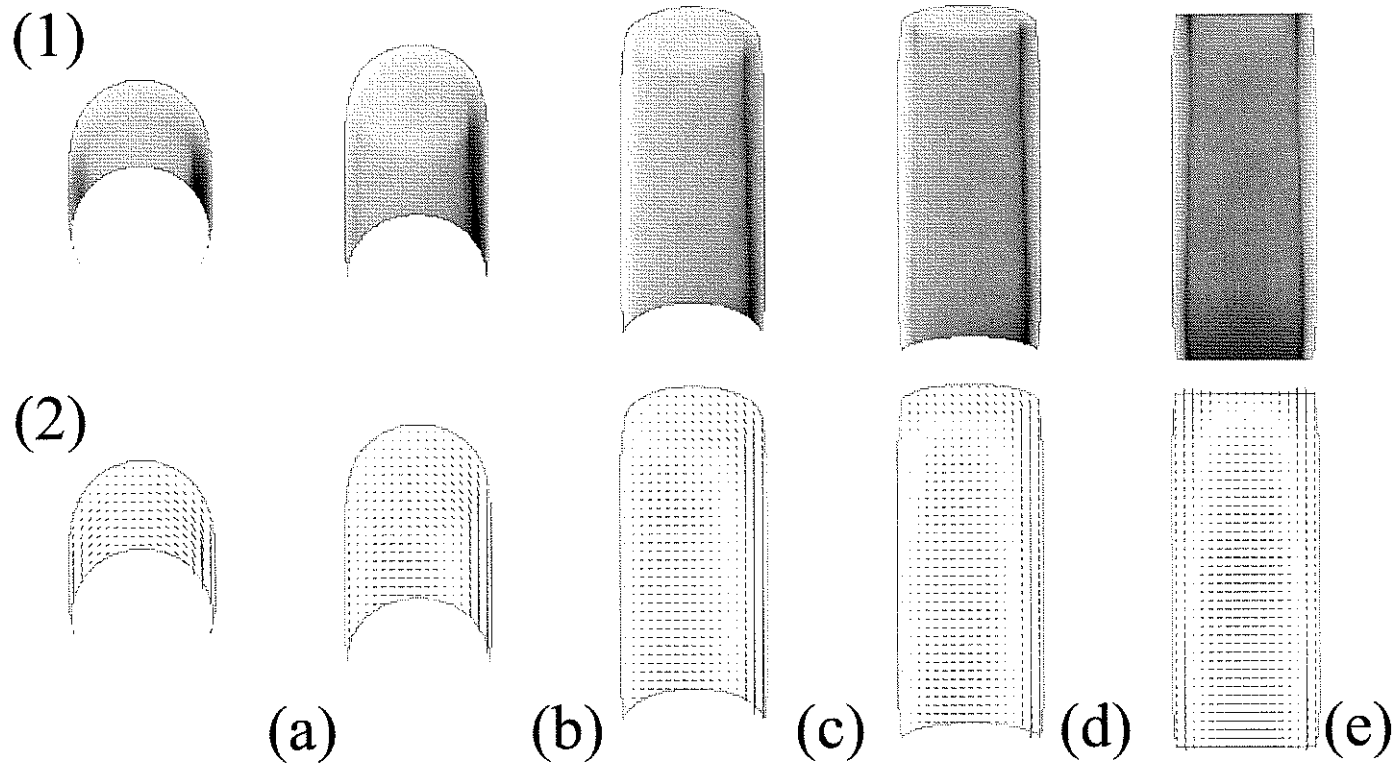

FIG. 5.—Calculated model counterparts for the total intensity and projected magnetic field in the case of the type-L–emitting region, when seen at (*a*) 15°, (*b*) 30°, (*c*) 60°, (*d*) 75°, and (*e*) 90° from the axis. Black in the gray scale indicates the maximum, and white indicates the minimum.

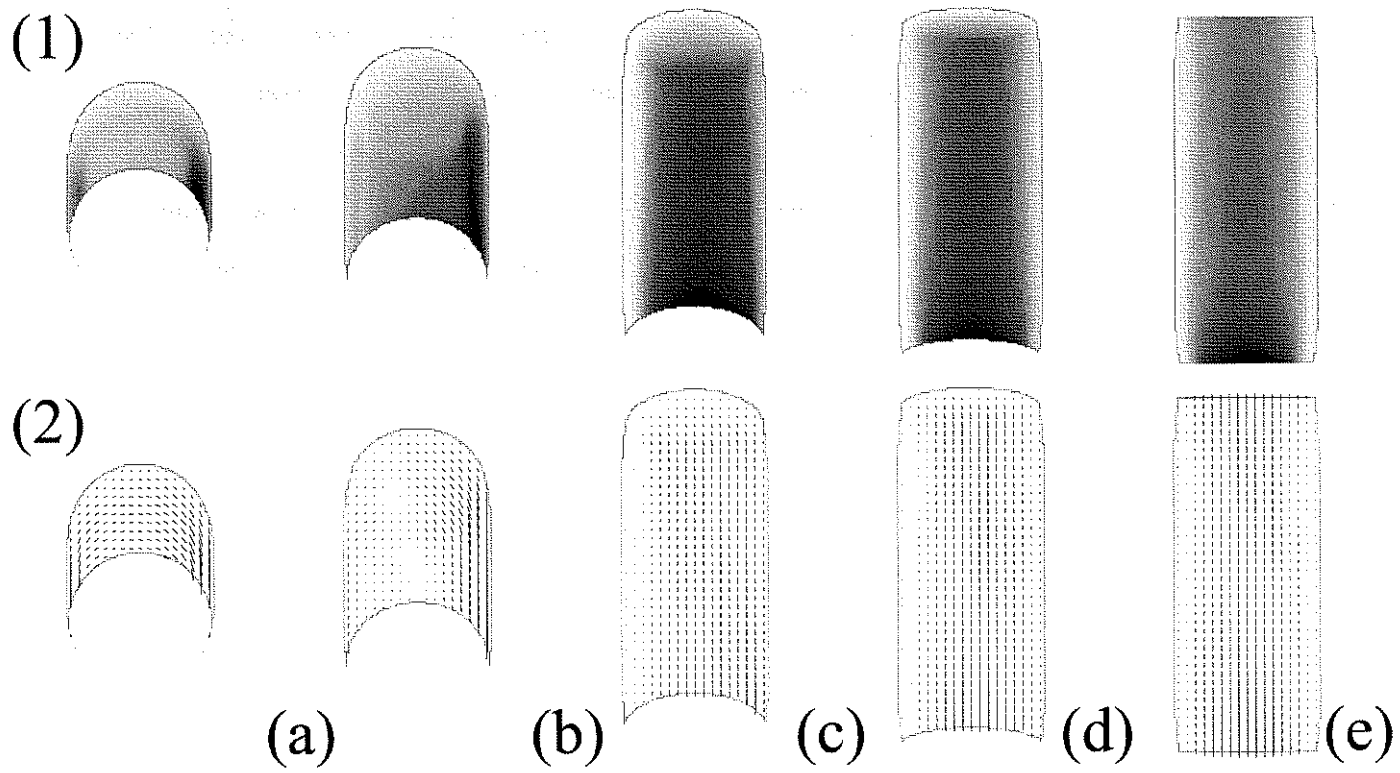

FIG. 6.—Calculated model counterparts for the total intensity and projected magnetic field in the case of the type-C–emitting region, when seen at (*a*) 15°, (*b*) 30°, (*c*) 60°, (*d*) 75°, and (*e*) 90° from the axis. Black in the gray scale indicates the maximum, and white indicates the minimum.

jets, using these results of our numerical observations, especially focusing on the FRM distribution.

Figure 7 shows a recent observational result for 3C 273 jet obtained by Asada et al. (2002) by using the VLBA Archive Data. In this case, the FRM distribution has a systematic gradient in the direction perpendicular to the jet axis, which can be interpreted as the sum of an antisymmetric distribution and a base value (a constant over the source).

It is not likely that the foreground magnetized cloud at a large distance from the jet has a very sharp variation of either the magnetic field or the density, just along the projected very thin jet (Taylor 1998; Asada et al. 2002). One likely interpretation may be that the antisymmetric contribution is due to the toroidal component of the helical magnetic field, as stated above. The base value may come from either the foreground large-scale magnetized clouds at large distances or the longitudinal component of the helical magnetic field. The latest observation of the 3C 273 jet shows that the systematic FRM gradient persists along a more significant length of the jet (K. Asada 2003, private communication), which would be a strong evidence for the above idea.

The projected magnetic field in 3C 273 is generally somewhat tilted from the axis of the jet, and the tilt angle becomes large at the blob called the "anomaly." Asada et al. (2002) attributed this to the shocks created on encountering nonuniformity. Another possibility is that the jet *is bent* at that point, so that the jet axis has less angle from the line of sight; the change of the FRM value can be explained with our model counterparts of different viewing angles [see the change, for example, from (*c*) to (*b*) in Fig. 4, row 1].

The observation of the jet from the AGN core of NGC 6251 (Perley et al. 1984) is shown in Figure 8. This may be a bit weaker evidence, but it is still considerably positive evidence for the systematic twist in the magnetic field. In this case, the contour lines of the FRM are nearly parallel in the central region up to 40″; therefore, the distribution of the FRM has a systematic antisymmetry with a gradient in the direction perpendicular to the jet axis, if we subtract the possible contribution from the spherically condensed gas cloud probably associated with the central part of the host galaxy. The projected magnetic field is aligned, and this would be consistent with the propagation of the TAWs.

The systematic and gradual change of the FRM value across the jet axis as seen in the preceding examples might suggest the existence of a helical magnetic field. In the MHD models, it is naturally explained as the results of the interaction between the large-scale magnetic field and the disk rotation. Nonmagnetic models may not be able to explain the FRM gradient. Although hydrodynamic models can include a magnetic field as a passive ingredient, the magnetic field in such a case is expected to be carried around passively by the motions of nonmagnetic gas dynamics. Such a passively distorted magnetic field will produce the Faraday depolarization, rather than showing clear systematic FRM distribution.

The FRM distribution, when the Faraday rotation occurs in the external medium around the jet, can be useful to determine the three-dimensional magnetic field structure around the jet, together with the projected magnetic field. We have demonstrated that the characteristic distribution of the FRM (systematic gradient perpendicular to the jet axis) in the straight part of some AGN jets can be explained by our "sweeping magnetic twist model." On the basis of this success, we are extending our numerical observation to the wiggled part of jets, which can be explained as a structural helix produced by MHD kink

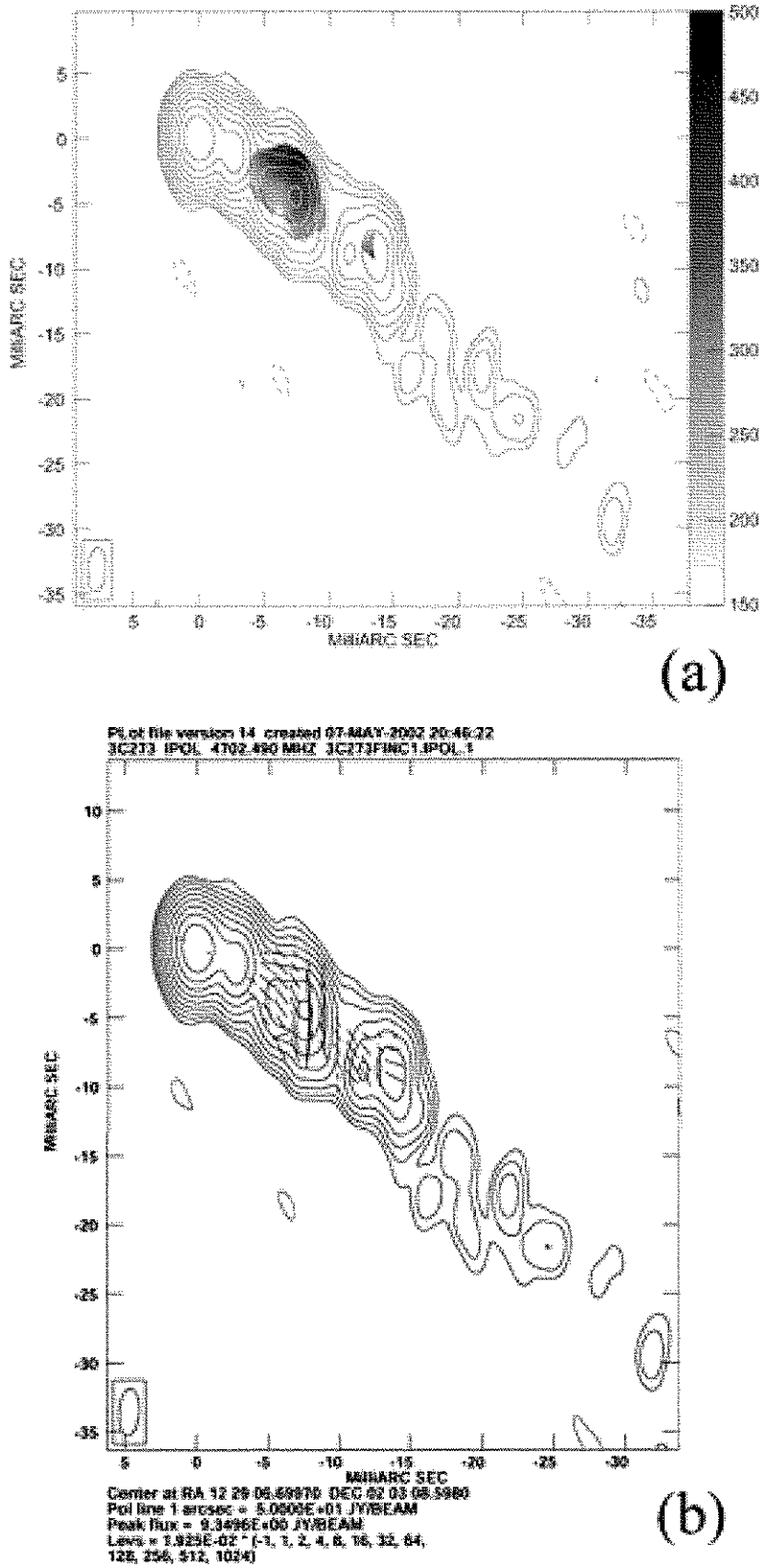

FIG. 7.—Distributions of (*a*) the Faraday rotation measure (this was modified from color to monochrome courtesy of the authors) and (*b*) the direction of projected magnetic field in the 3C 273 jet (Asada et al. 2002).

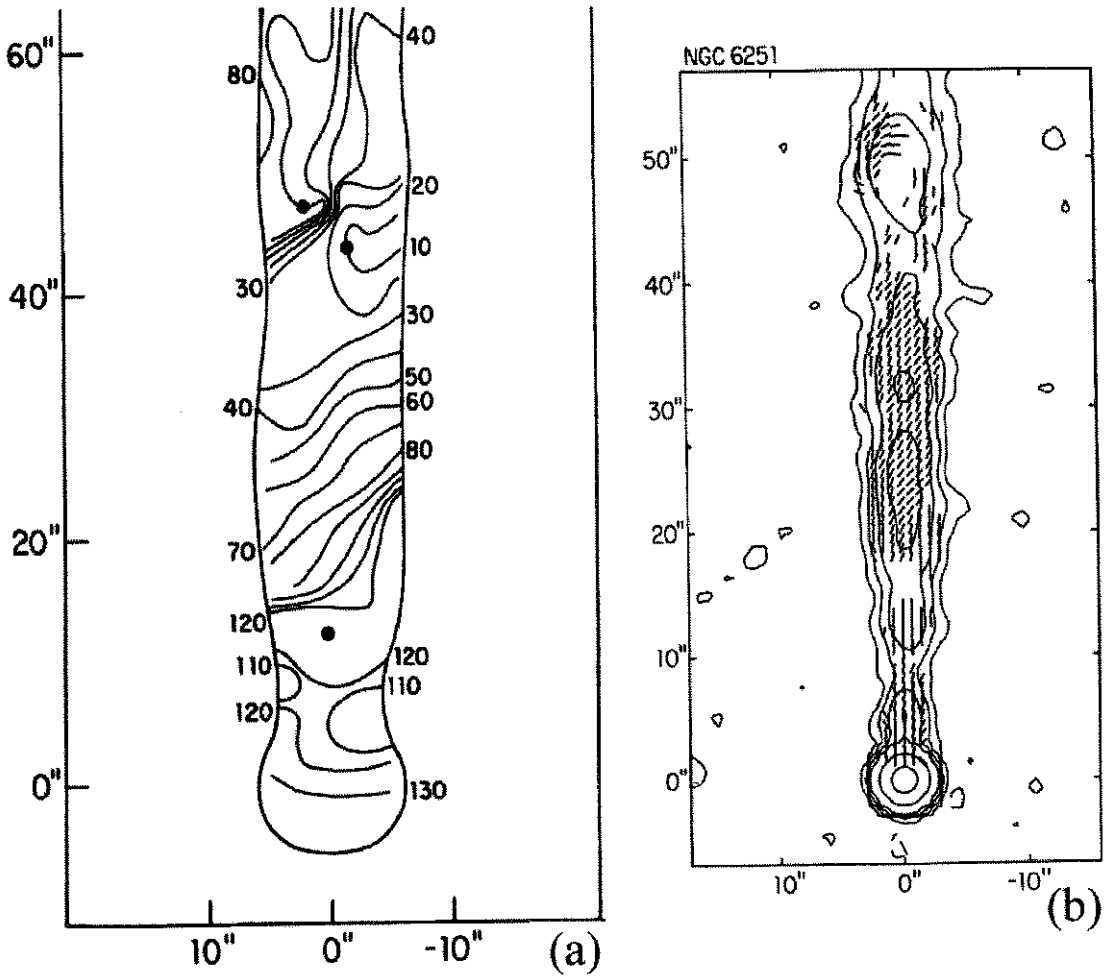

FIG. 8.—Distributions of (*a*) the Faraday rotation measure and (*b*) the direction of projected magnetic field in the NGC 6251 jet (Perley et al. 1984)

instability in the regime of our model (Nakamura et al. 2001). The results will be reported in an upcoming paper.

We acknowledge K. Asada for providing their precious results of the FRM distribution and M. Inoue for discussion. We hope that more observations of the FRM distribution in AGN jets will be performed in the near future, since they are very important in determining the correct theoretical model. Numerical computations were carried out on VPP5000, at the Astronomical Data Analysis Center of the National Astronomical Observatory, Japan, which is an inter-university research institute of astronomy, operated by the Ministry of Education, Culture, Sports, Science, and Technology.

REFERENCES

Asada, K., Inoue, M., Uchida, Y., Kameno, S., Fujisawa, K., Iguchi, S., & Mutoh, M. 2002, PASJ, 54, L39
Biretta, J. A., Owen, F. N., & Hardee, P. E. 1983, ApJ, 274, L27
Blandford, R. D. 1976, MNRAS, 176, 465
Blandford, R. D., & Payne, D. G. 1982, MNRAS, 199, 883
Burn, B. J. 1966, MNRAS, 133, 67
Clarke, D. A., Burns, J. O., & Feigelson, E. D. 1986, ApJ, 300, L41
Clarke, D. A., Norman, M. L., & Burns, J. O. 1989, ApJ, 342, 700
Eilek, J. A., & Owen, F. N. 2002, ApJ, 567, 202
Feretti, L., Perley, R., Giovannini, G., & Andernach, H. 1999, A&A, 341, 29
Hardee, P. E., & Rosen, A. 1999, ApJ, 524, 650
———. 2002, ApJ, 576, 204
Junor, W., Biretta, J. A., & Livio, M. 1999, Nature, 401, 891
Koide, S., Shibata, K., & Kudoh, T. 1998, ApJ, 495, L63
Kudoh, T., Matsumoto, R., & Shibata, K. 1998, ApJ, 508, 186
Kudoh, T., & Shibata, K. 1997a, ApJ, 474, 362
Kudoh, T., & Shibata, K. 1997b, ApJ, 476, 632
Laing, R. A. 1981, ApJ, 248, 87
Lovelace, R. V. E. 1976, Nature, 262, 649
Matsumoto, R., Uchida, Y., Hirose, S., Shibata, K., Hayashi, M., Ferrari, A., Bodo, G., & Norman, C. 1996, ApJ, 461, 115
Meier, D. L., Koide, S., & Uchida, Y. 2001, Science, 291, 84
Nakamura, M., Uchida, Y., & Hirose, S. 2001, NewA, 6, 61
Ouyed, R., & Pudritz, R. E. 1997, ApJ, 482, 712
Perley, R. A., Bridle, A. H., & Willis, A. G. 1984, ApJS, 54, 291
Stone, J. M., & Norman, M. L. 1994, ApJ, 433, 746
Taylor, G. B. 1998, ApJ, 506, 637
Uchida, Y., Nakamura, M., Hirose, S., & Uemura, S. 1999, Ap&SS, 264, 195
Uchida, Y., & Shibata, K. 1985, PASJ, 37, 515
———. 1986, Canadian J. Phys., 64, 507
Ustyugova, G. V., Koldoba, A. V., Romanova, M. M., Chechetkin, V. M., & Lovelace, R. V. E. 1995, ApJ, 439, L39